JACS
JOURNAL OF THE AMERICAN CHEMICAL SOCIETY

Article

pubs.acs.org/JACS

Interconversion between Superatomic 6-Electron and 8-Electron Configurations of M@$Au_{24}(SR)_{18}$ Clusters (M = Pd, Pt)

Kyuju Kwak,[†] Qing Tang,[‡] Minseok Kim,[†] De-en Jiang,*[,‡] and Dongil Lee*[,†]

[†]Department of Chemistry, Yonsei University, Seoul 120-749, Korea

[‡]Department of Chemistry, University of California, Riverside, California 92508, United States

Supporting Information

ABSTRACT: The exceptional stability of thiolate-protected Au_{25} clusters, $[Au_{25}(SR)_{18}]^-$, arises from the closure of superatomic electron shells, leading to a noble-gas-like 8-electron configuration ($1S^21P^6$). Here we present that replacing the core Au atom with Pd or Pt results in stable $[MAu_{24}(SR)_{18}]^0$ clusters (M = Pd, Pt) having a superatomic 6-electron configuration ($1S^21P^4$). Voltammetric studies of $[PdAu_{24}(SR)_{18}]^0$ and $[PtAu_{24}(SR)_{18}]^0$ reveal that the highest occupied molecular orbital–lowest unoccupied molecular orbital (HOMO–LUMO) gaps of these clusters are 0.32 and 0.29 eV, respectively, indicating their electronic structures are drastically altered upon doping of the foreign metal. Density functional investigations confirm that the HOMO–LUMO gaps of these clusters are indeed smaller, respectively 0.33 and 0.32 eV, than that of $[Au_{25}(SR)_{18}]^-$ (1.35 eV). Analysis of the optimized geometries for the 6-electron $[MAu_{24}(SR)_{18}]^0$ clusters shows that the MAu_{12} core is slightly flattened to yield an oblate ellipsoid. The drastically decreased HOMO–LUMO gaps observed are therefore the result of Jahn–Teller-like distortion of the 6-electron $[MAu_{24}(SR)_{18}]^0$ clusters, accompanying splitting of the 1P orbitals. These clusters become 8-electron $[MAu_{24}(SR)_{18}]^{2-}$ clusters upon electronic charging, demonstrating reversible interconversion between the 6-electron and 8-electron configurations of $MAu_{24}(SR)_{18}$.

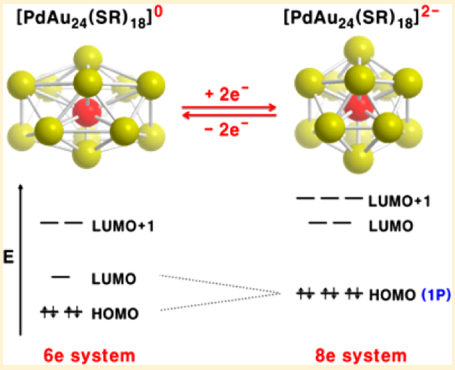

INTRODUCTION

Thiolate-protected gold clusters have attracted significant research interest recently because of promises offered by their unique catalytic, optical, and electrochemical properties.[1−4] These clusters have special stability at certain compositions, and thus, atomically precise clusters are typically obtained from a variety of size-selective syntheses.[3−5] Among the gold clusters reported, the $Au_{25}(thiolate)_{18}$ cluster has been the most extensively studied system. X-ray crystallographic analysis showed that it consists of a centered icosahedral Au_{13} core protected with six $Au_2(thiolate)_3$ motifs.[6−9] The exceptional stability of the anionic $[Au_{25}(thiolate)_{18}]^-$ was explained by the electronically closed shell superatom model.[10,11] In this model, the number of superatomic electrons, n^*, for approximately spherical thiolate-protected metal (M) clusters, $[M_N(thiolate)_L]^z$, is given by

$$n^* = NV_A - L - z \quad (1)$$

where V_A is the valence of the metal atom. For $[Au_{25}(thiolate)_{18}]^-$ clusters, $n^* = (25 \times 1) - 18 - (-1) = 8$. These 8 electrons fully fill the 1S(2e) and 1P(6e) levels of the superatomic electron shell ($1S^21P^6$), and thus, $Au_{25}(thiolate)_{18}$ is thought to be most stable with an oxidation state of −1.

In comparative optical studies of Au_{25} clusters using experimental and computational methods, Jin and co-workers[7] showed that the first absorption peak at ∼1.8 eV corresponds to a highest occupied molecular orbital–lowest unoccupied molecular orbital (HOMO–LUMO) transition in the Au_{13} core. This absorption peak has been found to be rather insensitive to the change in the ligand shell surrounding the gold core.[12−14] In addition, there have been a number of electrochemical studies which have proven to be powerful in unraveling the electronic structure near HOMO–LUMO levels of gold clusters.[1] While there have been some ligand effects observed in the voltammetry of Au_{25} clusters,[14−17] the HOMO–LUMO energy gaps of Au_{25} clusters predicted from voltammetry of Au_{25} clusters were found to be ∼1.33 V regardless of the thiolate ligands.[1,9,14,15]

Whereas the optical and electrochemical properties of Au_{25} clusters are rather insensitive to the change in the ligand shell, they are likely to respond more sensitively to the change in core composition. Therefore, replacing the core gold with a foreign metal may open a new avenue to the fine-tuning of the cluster properties.[18−25] Murray and co-workers[26] first reported that mono-Pd-doped $PdAu_{24}(SC_2H_4Ph)_{18}$ clusters were observed in a mixture with $Au_{25}(SC_2H_4Ph)_{18}$ clusters in mass spectra. Negish et al.[27] managed to isolate highly pure $PdAu_{24}(SC_{12}H_{25})_{18}$ clusters using solvent fractionation and high-performance liquid chromatography (HPLC). Density functional theory (DFT) calculations on the $PdAu_{24}$ cluster system have predicted that the center-doped $PdAu_{24}$ cluster is the most

Received: July 4, 2015
Published: July 29, 2015

DOI: 10.1021/jacs.5b06946
J. Am. Chem. Soc. 2015, 137, 10833−10840

stable form.[28,29] The center-doped $PdAu_{24}$ cluster was experimentally confirmed by using the combination of ^{197}Au Mössbauer and extended X-ray absorption fine-structure (EXAFS) spectroscopy.[30]

In addition to Pd, a Au_{25} cluster doped with Pt is another interesting cluster system, especially for various technological applications. Jiang et al.[28] performed an in silico screening of center-doped $M@Au_{24}$ clusters by using the DFT calculations and predicted that both Pd-doped and Pt-doped Au_{25} clusters are highly stable and possess even higher interaction energy between the central dopant (M) and the surrounding $Au_{24}(thiolate)_{18}$ framework than the homogold system. On the basis of the high stability of the $PtAu_{24}$ cluster, Jin et al.[31] successfully isolated neutral $[PtAu_{24}(SC_2H_4Ph)_{18}]^0$ clusters by separating $PtAu_{24}(SC_2H_4Ph)_{18}$ clusters using size-exclusion chromatography (SEC) after decomposing the $Au_{25}(SC_2H_4Ph)_{18}$ cluster in the product mixture. By simulating the optical absorption spectra of $[PtAu_{24}(SCH_3)_{18}]^0$ clusters, they found the Pt doping at the center of the cluster gave the best fit with the experimental spectrum. The central doping of the $PtAu_{24}$ cluster was also confirmed by Zhang et al.[32] using element-specific X-ray spectroscopy methods.

It is now well established that Pd and Pt dopants are preferentially located at the center of the core, and the doped clusters are found to be charge neutral, i.e., $[PdAu_{24}(thiolate)_{18}]^0$ and $[PtAu_{24}(thiolate)_{18}]^0$, as opposed to the 8-electron systems, such as $[PdAu_{24}(thiolate)_{18}]^{2-}$ and $[PtAu_{24}(thiolate)_{18}]^{2-}$, that are predicted from the superatom model.[27,30−32] What is the origin of the stability for $[PdAu_{24}(thiolate)_{18}]^0$ and $[PtAu_{24}(thiolate)_{18}]^0$ that are preferably obtained in the synthesis then? This has motivated us to investigate the electronic structures of the synthesized $PdAu_{24}(SR)_{18}$ and $PtAu_{24}(SR)_{18}$ clusters, where SR is 1-hexanethiolate, using voltammetric methods. Very clean voltammograms were obtained, which were distinctively different from that of $Au_{25}(SR)_{18}$. The HOMO−LUMO gaps of $PdAu_{24}(SR)_{18}$ and $PtAu_{24}(SR)_{18}$ deduced from the voltammograms were quite similar, but considerably smaller than that of $Au_{25}(SR)_{18}$, suggesting that their electronic structures were significantly altered by doping of the foreign metal. These results were strongly supported by DFT calculations, which also suggested a possible geometrical distortion occurring in the doped clusters. Finally, reversible interconversions between the superatomic 6-electron and 8-electron configurations are demonstrated by spectroelectrochemistry of $PdAu_{24}(SR)_{18}$, $PtAu_{24}(SR)_{18}$, and $Au_{25}(SR)_{18}$.

EXPERIMENTAL SECTION

Syntheses of $Au_{25}(SR)_{18}$, $PtAu_{24}(SR)_{18}$, and $PdAu_{24}(SR)_{18}$ Clusters. Detailed synthetic procedures and characterizations of $Au_{25}(SR)_{18}$, $PtAu_{24}(SR)_{18}$, and $PdAu_{24}(SR)_{18}$ are provided in the Supporting Information.

Electrochemistry and Spectroelectrochemistry. Voltammetry was carried out with an electrochemical workstation (model 660 B, CH Instruments) in CH_2Cl_2, containing 0.1 M tetrabutylammonium hexafluorophosphate (Bu_4NPF_6) as a supporting electrolyte, that was degassed and blanketed with a high-purity Ar gas. Square wave voltammetry (SWV) was conducted at 100 mV/s with a pulse height and a width of 20 mV and 20 ms, respectively. A Pt disk (0.4 mm diameter) was used as the working electrode, a Pt disk (0.4 mm diameter) as the counter electrode, and a Ag wire quasi-reference electrode (AgQRE) as the reference electrode for the voltammetric measurements. Ferrocene ($Fc^{+/0}$) was added as an internal reference for AgQRE. In this paper, potentials are reported versus $Fc^{+/0}$. Reduced temperature voltammetry was conducted using cold baths of acetone/dry ice (−78 °C).

In situ spectroelectrochemical experiments were performed in a rectangular quartz spectrophotometric cuvette with a 2 mm light path (104.002F-QS, Hellma). The working electrode was a Pt mesh that sat within the optical path of the spectrometer. A AgQRE and a Pt wire counter electrode were used. The cluster solution was 0.5 mM CH_2Cl_2, containing 0.1 M Bu_4NPF_6, that was degassed and blanketed with a high-purity Ar gas. The solution also contained 10.0 mM *tert*-butylamine borane (TBAB) and 1.0 mM tetraoctylammonium bromide (Oct_4NBr), which were added to stabilize the reduced $[PdAu_{24}(SR)_{18}]^{2-}$ ($[PtAu_{24}(SR)_{18}]^{2-}$) clusters produced during potentiostatic reduction.

Computational Methods. DFT calculations of the $Au_{25}(SR)_{18}$, $PdAu_{24}(SR)_{18}$, and $PtAu_{24}(SR)_{18}$ clusters were all performed with the quantum chemistry program Turbomole V6.5.[33] To save the computational time, we simplified the R groups with $-CH_3$ groups. The def2-SV(P) basis sets were used for C, S, and H, while effective core potentials which include scalar relativistic corrections and 19 (18) valence electrons were used for Au (Pd, Pt).[34] Geometry optimization was done with the TPSS (Tao, Perdew, Staroverov, and Scuseria) functional.[35] Time-dependent DFT (TD-DFT) calculations were done at the B3-LYP level with def2-SV(P) basis sets. All transitions together with their oscillator strengths were then convoluted with a Lorentzian line shape of 0.15 eV broadening to make the optical-absorption spectrum.

RESULTS AND DISCUSSION

Figure 1 shows the positive-mode matrix-assisted laser desorption ionization (MALDI) mass spectra of the isolated

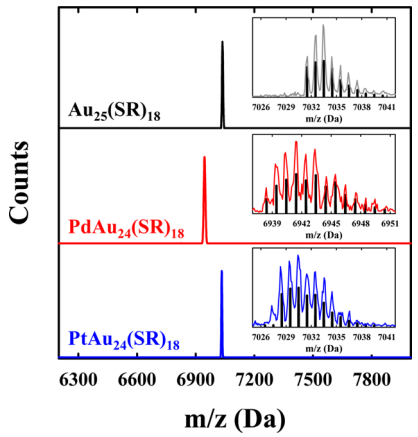

Figure 1. MALDI mass spectra of $Au_{25}(SR)_{18}$ (black), $PdAu_{24}(SR)_{18}$ (red), and $PtAu_{24}(SR)_{18}$ (blue). The insets show the comparisons between the experimental data (lines) and the simulated isotope patterns (black bars).

$Au_{25}(SR)_{18}$ (black), Pd-doped (red), and Pt-doped (blue) gold clusters. As can be seen in the figure, there is only a single peak observed for each cluster, indicating that the isolated clusters are highly pure. As compared in the inset (red), the observed peaks at $m/z \sim 6943$ match well with the simulated isotope pattern of $PdAu_{24}(SR)_{18}$, which are well separated from the peak (~7034 Da) of the intact $Au_{25}(SR)_{18}$. The peak at ~7032 Da observed for the Pt-doped gold cluster is, however, almost superimposed with that of $Au_{25}(SR)_{18}$ because of their small mass difference (1.89 Da). However, the isotope pattern of the Pt-doped cluster (blue) matches well with the simulated isotope pattern of $PtAu_{24}(SR)_{18}$, which can be clearly distinguished from that of $Au_{25}(SR)_{18}$ (black) as shown in the insets of Figure 1.

DOI: 10.1021/jacs.5b06946
J. Am. Chem. Soc. 2015, 137, 10833−10840

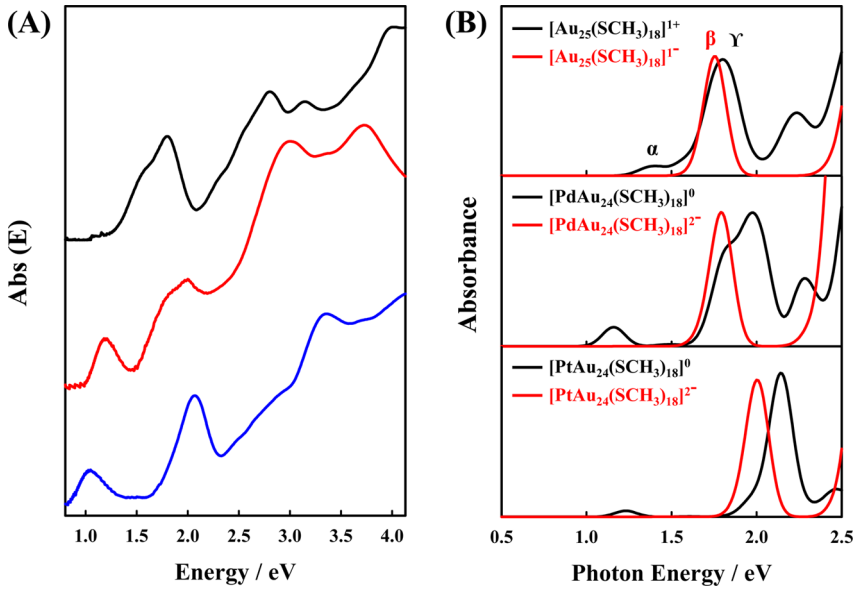

Figure 2. (A) UV−vis−NIR absorption spectra of $Au_{25}(SR)_{18}$ (black), $PdAu_{24}(SR)_{18}$ (red), and $PtAu_{24}(SR)_{18}$ (blue) clusters in trichloroethylene. The wavelength-scale absorption spectrum, Abs(λ), was converted to the energy-scale spectrum, Abs(E), according to the relation Abs(E) $\propto$ [Abs(λ)]λ^2. (B) TD-DFT-simulated optical spectra of $Au_{25}(SCH_3)_{18}$ (top), $PdAu_{24}(SCH_3)_{18}$ (middle), and $PtAu_{24}(SCH_3)_{18}$ (bottom) possessing 6 (black) and 8 (red) superatomic electrons.

X-ray photoelectron spectroscopy (XPS) analysis was carried out to gain further insight into the isolated $PdAu_{24}(SR)_{18}$ and $PtAu_{24}(SR)_{18}$ clusters. Figure S1A shows the Au 4f XPS spectra of $Au_{25}(SR)_{18}$, $PdAu_{24}(SR)_{18}$, and $PtAu_{24}(SR)_{18}$. The $4f_{7/2}$ peak is found at 83.8 eV for $Au_{25}(SR)_{18}$ and shows a negative shift of 0.11 and 0.17 eV for $PdAu_{24}(SR)_{18}$ and $PtAu_{24}(SR)_{18}$, respectively. This shift may arise from the internal charge transfer from the less electronegative Pd (Pt) heteroatom to the more electronegative Au atoms.[30,36,37] Similar negative shifts have been observed for Pt-doped and Ag-doped Au_{25} clusters.[18,32] The Pd 3d and Pt 4f XPS peaks are clearly observed in parts B and C, respectively, of Figure S1. Normalization of the XPS peaks by their relative elemental sensitivity factors yielded average compositions of $Pd_{1.0}Au_{24.0}$ and $Pt_{0.9}Au_{24.1}$, in good agreement with those determined by mass spectrometry (Figure 1). In addition, the Pd $3d_{3/2}$ XPS peak observed at 341.4 eV, which corresponds to Pd^0, suggests that Pd atom is located at the center of $PdAu_{24}(SR)_{18}$; a positive shift would be expected if it was located at the surface of the core or in the ligand shell.[19,32,38] Similarly, the Pt $4f_{5/2}$ and $4f_{7/2}$ peaks observed at respectively 75.1 and 71.8 eV suggest that the doped Pt atom is located at the center of $PtAu_{24}(SR)_{18}$.[32] Transmission electron microscopy (TEM) images of the isolated $PdAu_{24}(SR)_{18}$ and $PtAu_{24}(SR)_{18}$ clusters in Figure S2 show that the average core sizes are both around 1.1 nm, similar to that of $Au_{25}(SR)_{18}$.

Both $PtAu_{24}(SR)_{18}$ and $PdAu_{24}(SR)_{18}$ clusters were synthesized according to the one-phase procedure reported by Jin and et al.[31] with some modifications. Details are provided in the Supporting Information. Briefly, in the synthesis of the $PtAu_{24}(SR)_{18}$ cluster 1-hexanethiol (RSH) was added to a 4:1 molar mixture of $HAuCl_4$ and H_2PtCl_6 dissolved in tetrahydrofuran to form metal−thiol aggregates, which then were reduced by $NaBH_4$ to produce metal clusters. A mixture of $Au_{25}(SR)_{18}$ and $PtAu_{24}(SR)_{18}$ clusters was typically produced in this synthesis. $PtAu_{24}(SR)_{18}$ was subsequently isolated by decomposing $Au_{25}(SR)_{18}$ selectively by reaction with concentrated H_2O_2. The $PdAu_{24}(SR)_{18}$ cluster was synthesized similarly by the one-phase procedure. $PdAu_{24}(SR)_{18}$ was also found to be very robust in the oxidation environment and thus could be isolated by selectively decomposing $Au_{25}(SR)_{18}$ with H_2O_2 in the mixture.

Evidently, the robustness of $PdAu_{24}(SR)_{18}$ ($PtAu_{24}(SR)_{18}$) in the oxidation environment is the enabling factor in isolating $PdAu_{24}(SR)_{18}$ from $Au_{25}(SR)_{18}$. However, there is also considerable loss of $PdAu_{24}(SR)_{18}$ observed when decomposing a large amount of $Au_{25}(SR)_{18}$ clusters in the mixture. To minimize the fraction of $Au_{25}(SR)_{18}$ in the mixture, clusters were synthesized with a shorter metal−thiol aggregation time (10 min) to reduce the production of $Au_{25}(SR)_{18}$; the highest $Au_{25}(SR)_{18}$ yield was typically achieved at ∼60 min of the Au−thiol aggregation time. As compared in the mass spectra shown in Figure S3A (red), it was found that the intensity of the peak (m/z 7034 Da) corresponding to the intact $Au_{25}(SR)_{18}$ was much higher than that corresponding to $PdAu_{24}(SR)_{18}$ (m/z 6943 Da) when the metal−thiol aggregation time was 60 min. By contrast, the relative yield of $PdAu_{24}(SR)_{18}$ to $Au_{25}(SR)_{18}$ increased significantly when the metal−thiol aggregation time was shortened to 10 min as can be seen in Figure S3A (black). The low production of $Au_{25}(SR)_{18}$ allows us to remove $Au_{25}(SR)_{18}$ completely from the mixture within 2 h of H_2O_2 treatment as shown in Figure S3B. Highly pure $PdAu_{24}(SR)_{18}$ ($PtAu_{24}(SR)_{18}$) clusters were then isolated by extracting them with a 2:1 (v/v) CH_3CN/CH_2Cl_2 mixture.

Figure 2A shows the UV−vis−NIR absorption spectra of $Au_{25}(SR)_{18}$ (black), $PdAu_{24}(SR)_{18}$ (red), and $PtAu_{24}(SR)_{18}$ (blue). The absorption profile is shown in the photon energy scale to see the broad NIR peak more clearly. The wavelength-scale absorption spectra are shown in Figure S4. The $Au_{25}(SR)_{18}$ clusters exhibit the characteristic absorption profile of the Au_{25} cluster with peaks at 1.8, 2.8, and 3.1 eV. Upon Pd doping, the absorption profile becomes significantly altered as can be seen in Figure 2A (red). That is, there are two absorption bands observed at 1.8 and 2.0 eV in the low-energy

DOI: 10.1021/jacs.5b06946
J. Am. Chem. Soc. 2015, 137, 10833−10840

Table 1. Formal Potentials (V vs $Fc^{+/0}$) and Potential Gaps (V) Observed in Figure 3

	O2	O1	R1	R2	O1−R1	HOMO−LUMO
$Au_{25}(SR)_{18}$	−0.04	−0.39	−2.06		1.67	1.32
$PdAu_{24}(SR)_{18}$	0.40	−0.03	−0.78	−1.10	0.75	0.32
$PtAu_{24}(SR)_{18}$	0.41	−0.03	−0.76	−1.10	0.73	0.29

region (<2.5 eV) with an additional NIR band centered at 1.2 eV. This spectrum matches very well with the TD-DFT-simulated spectrum that focuses on the NIR to visible region (1.0−2.5 eV). From Figure 2B (middle, black), one can see that TD-DFT can indeed reproduce the peak at ∼1.2 eV and the peaks between 1.75 and 2.0 eV, manifesting that the isolated Pd-doped cluster is center-doped $[PdAu_{24}(SCH_3)_{18}]^0$. While the visible absorption peaks at 1.8 and 2.0 eV are in good agreement with those reported for the center-doped $PdAu_{24}(SR)_{18}$, the NIR peak at 1.2 eV has not been observed before,[22,23,25] presumably due to insufficient instrumental sensitivity in the NIR region in the previous studies. By employing a UV−vis−NIR spectrometer and trichloroethylene as a clean solvent with a low background, the NIR peak could be clearly observed in the present work.

In Figure 2A, the absorption profile of $PtAu_{24}(SR)_{18}$ is also found to be significantly different from that of $Au_{25}(SR)_{18}$. That is, there is a strong absorption band found at 2.1 eV with an additional NIR band centered at 1.1 eV in the low-energy region. This absorption profile matches well with that reported for the $PtAu_{24}(SR)_{18}$ cluster.[31] Again, this spectrum agrees well with the one simulated for the center-doped $[PtAu_{24}(SCH_3)_{18}]^0$ as shown in Figure 2B (bottom, black). While both absorption profiles of $PdAu_{24}(SR)_{18}$ and $PtAu_{24}(SR)_{18}$ are significantly different from that of $Au_{25}(SR)_{18}$, they are rather similar to each other, especially in the low-energy region (<2.5 eV). The similarity in absorption spectra may indicate that they adopt similar electronic structures (vide infra).

To further unravel the electronic structure of Pd- and Pt-doped clusters, we carried out SWVs of CH_2Cl_2 solutions of $Au_{25}(SR)_{18}$ (black), $PdAu_{24}(SR)_{18}$ (red), and $PtAu_{24}(SR)_{18}$ (blue) clusters at room temperature. Voltammetric measurements of metal clusters have proven to be a powerful means of investigating the electronic energy structure near the HOMO−LUMO levels.[1] For the precise comparison, measured potentials were corrected using ferrocene ($Fc^{+/0}$) as an internal standard. The redox potentials observed in SWVs are listed in Table 1. In Figure 3, the SWVs display well-resolved current peaks that lie at the formal potentials of the cluster charge-state couples. We note that the voltammogram of the $PdAu_{24}(SR)_{18}$ cluster has been reported before, although the current peaks were not clearly resolved.[26,27] The voltammogram of $PtAu_{24}(SR)_{18}$ reported here is the first one to our knowledge. For the $Au_{25}(SR)_{18}$ cluster, the open-circuit potential (OCP) was found at −0.49 V, indicating that the $Au_{25}(SR)_{18}$ cluster is in anionic form, i.e., $[Au_{25}(SR)_{18}]^-$. There are three oxidation peaks observed at −0.39 (O1), −0.04 (O2), and 0.69 (O3) and one reduction peak at −2.06 V (R1) in the potential range investigated. The electrochemical gap determined from the difference between the first oxidation (O1) and reduction (R1) potentials is found to be 1.67 V. Subtracting the charging energy, which is typically estimated using the gap between O1 and O2 (0.35 V), from the O1−R1 gap gives a corrected energy of 1.32 eV, which constitutes an electrochemical prediction of the HOMO−LUMO gap for $Au_{25}(SR)_{18}$.[1,9,14,15] The predicted

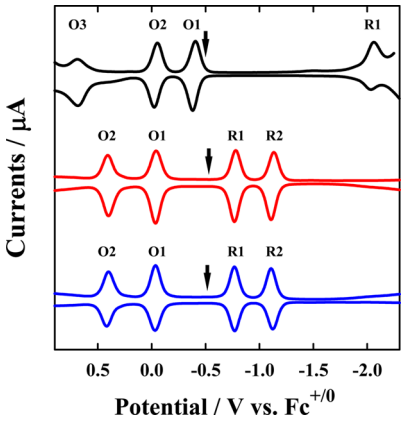

Figure 3. SWVs of $Au_{25}(SR)_{18}$ (black), $PdAu_{24}(SR)_{18}$ (red), and $PtAu_{24}(SR)_{18}$ (blue). The electrochemical measurements were performed in CH_2Cl_2 containing 0.1 M Bu_4NPF_6. The arrows indicate solution OCPs.

HOMO−LUMO gap matches very well with the calculated one (1.35 eV, Table 2) for $[Au_{25}(SCH_3)_{18}]^-$.

In Figure 3, the $PdAu_{24}(SR)_{18}$ cluster shows a voltammogram drastically different from that of $Au_{25}(SR)_{18}$. That is, there is a doublet of oxidation at −0.03 (O1) and 0.40 (O2) and a doublet of reduction at −0.78 (R1) and −1.10 V (R2) with the OCP found at −0.48 V. Unlike the $Au_{25}(SR)_{18}$ cluster that is isolated in the anionic form along with the tetraoctylammonium (Oct_4N^+) counterion, there is no Oct_4N^+ found in the isolated $PdAu_{24}(SR)_{18}$ as confirmed by NMR spectroscopy shown in Figure S5. In addition, the OCP of $PdAu_{24}(SR)_{18}$ is found at −0.48 V in the middle of doublets in the voltammogram. This evidently indicates that the isolated $PdAu_{24}(SR)_{18}$ is a neutral cluster, the oxidation doublet observed in Figure 3 corresponds to $[PdAu_{24}(SR)_{18}]^{1+/0}$ (O1) and $[PdAu_{24}(SR)_{18}]^{2+/1+}$ (O2), and the reduction doublet corresponds to $[PdAu_{24}(SR)_{18}]^{0/1-}$ (R1) and $[PdAu_{24}(SR)_{18}]^{1-/2-}$ (R2). The combination of voltammetry and NMR analysis clearly confirms that the isolated $PdAu_{24}(SR)_{18}$ has a *zero* charge state, not a −2 charge state, as opposed to the prediction from the superatom model (vide infra). Voltammetry was also conducted at −78 °C (Figure S6), which shows an additional oxidation peak (O3) corresponding to the $[PdAu_{24}(SR)_{18}]^{3+/2+}$ wave at ∼1.00 V. The formal potentials and potential gaps observed in Figure S6 are given in Table S1. Whereas the O3 peak becomes unresolved at room temperature, the oxidation doublet (O1 and O2) and the reduction doublet (R1 and R2) remain well resolved, indicating that the oxidation and reduction reactions of $PdAu_{24}(SR)_{18}$ are chemically reversible. The electrochemical gap between O1 and R1 is found to be 0.75 V. Taking into account the charging energy (0.43 V) from Table 1, (O1−O2) gives a HOMO−LUMO gap of 0.32 V, which is dramatically decreased from 1.32 V by replacing the central Au with a Pd atom in the cluster. Interestingly, this value agrees very well with the calculated HOMO−LUMO gap (0.33 eV, Table 2) for the center-doped $[PdAu_{24}(SCH_3)_{18}]^0$, showing that voltammetry is

DOI: 10.1021/jacs.5b06946
J. Am. Chem. Soc. 2015, 137, 10833−10840

Table 2. Calculated HOMO−LUMO Gaps and Flattening Factors (f) for $Au_{25}(SCH_3)_{18}$, $PdAu_{24}(SCH_3)_{18}$, and $PtAu_{24}(SCH_3)_{18}$ Possessing 6 and 8 Superatomic Electrons

	8-electron system			6-electron system		
	$[Au_{25}(SCH_3)_{18}]^-$	$[PdAu_{24}(SCH_3)_{18}]^{2-}$	$[PtAu_{24}(SCH_3)_{18}]^{2-}$	$[Au_{25}(SCH_3)_{18}]^+$	$[PdAu_{24}(SCH_3)_{18}]^0$	$[PtAu_{24}(SCH_3)_{18}]^0$
HOMO−LUMO gap[a] (eV)	1.35	1.41	1.60	0.39	0.33	0.32
f[b]	0.003	0.001	0.002	0.026	0.026	0.023

[a]The HOMO−LUMO gaps are calculated at the TPSS/def2(SV(P) level. [b]The flattening factor (f) is defined as $(a - b)/a$, where a and b are radii along the major and minor axes of the oblate ellipsoid.

indeed powerful in the determination of the electronic structure of a cluster near the HOMO−LUMO levels.

The SWV of $PtAu_{24}(SR)_{18}$ also exhibits a similar pattern with a doublet of oxidation at −0.03 (O1) and 0.41 (O2) and a doublet of reduction at −0.76 (R1) and −1.10 V (R2) with the OCP found at −0.49 V. $PtAu_{24}(SR)_{18}$ is also found to be neural, and the voltammetric peaks can be assigned similarly. The observed O1−R1 gap and the deduced HOMO−LUMO gaps from the SWV (Figure 3) are determined to be 0.73 and 0.29 V, respectively. Again, this value agrees very well with the calculated HOMO−LUMO gap (0.32 eV, Table 2) for the center-doped $[PtAu_{24}(SCH_3)_{18}]^0$. These voltammetry results clearly indicate that the electronic structure of $Au_{25}(SR)_{18}$ is significantly altered by doping of Pd (Pt), and the resulting $PdAu_{24}(SR)_{18}$ and $PtAu_{24}(SR)_{18}$ clusters adopt quite similar electronic structures.

To corroborate the voltammetric results in Figure 3, we simulated the energy levels of 6-electron and 8-electron systems as depicted in Figure 4. As reported before, the high stability of

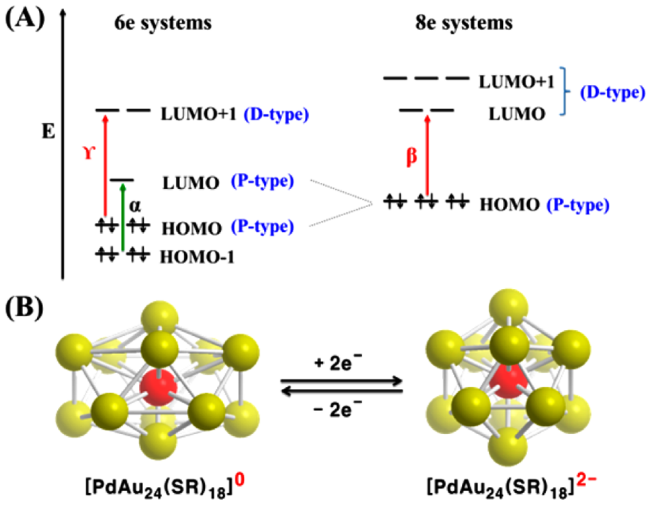

Figure 4. (A) Electronic energy levels of 6-electron and 8-electron systems. α, β, and γ denote the optical transitions occurring in the 6-electron and 8-electron systems. (B) Cartoon depicting Jahn−Teller-like distortion in the core (e.g., $PdAu_{12}$) predicted for the 6-electron $[PdAu_{24}(SR)_{18}]^0$ (left), which undergoes a structural change to nearly spherical 8-electron $[PdAu_{24}(SR)_{18}]^{2-}$ upon reduction (right). The vertical compression for $[PdAu_{24}(SR)_{18}]^0$ (left) is exaggerated.

$[Au_{25}(SR)_{18}]^-$ has been explained by the electronically closed-shell superatom model.[10,11] The 8 electrons fully fill the 1S(2e) and 1P(6e) levels of the superatomic electron shell ($1S^21P^6$). DFT calculations have shown that the HOMO level is triply degenerate 1P orbitals while the LUMO is doubly degenerate 1D orbitals with a HOMO−LUMO gap of 1.35 eV (Table 2). Considering the superatom model for $PdAu_{24}(SR)_{18}$, one would expect that $[Au_{25}(SR)_{18}]^-$ and $[PdAu_{24}(SR)_{18}]^{2-}$ are isoelectronic in that they have the same 8-electron configuration. The neutral 6-electron $[PdAu_{24}(SR)_{18}]^0$ identified in this work possesses two less electrons than $[Au_{25}(SR)_{18}]^-$, and the triply degenerate HOMO would split into a doubly degenerate HOMO and LUMO, both of which show the character of the superatomic 1P orbital as portrayed in Figure 4. The HOMO−LUMO gaps of 6-electron and 8-electron systems are summarized in Table 2.

The splitting of the 1P orbitals has the same physical origin as the Jahn−Teller distortion, to remove degeneracy. Indeed, we found from the optimized geometries that the 8-electron systems such as $[Au_{25}(SCH_3)_{18}]^-$, $[PdAu_{24}(SCH_3)_{18}]^{2-}$, and $[PtAu_{24}(SCH_3)_{18}]^{2-}$ have a nearly spherical-like icosahedral 13-atom core, while for the 6-electron systems, $[Au_{25}(SCH_3)_{18}]^+$, $[PdAu_{24}(SCH_3)_{18}]^0$, and $[PtAu_{24}(SCH_3)_{18}]^0$, the core is slightly flattened to yield an oblate ellipsoid (the flattening factor is about 0.026, Table 2). This is certainly related to the superatomic orbitals of the 6-electron systems, as now $(1P_{x,y})^4$ is the HOMO, while $1P_z$ is the LUMO. The flattened axis (that is, the minor axis) is where $1P_z$ lies, so its energy becomes higher.

From Figure 2B, one can see that TD-DFT can indeed reproduce (1) the peak between 1.0 and 1.5 eV (α) for the three 6-electron systems and (2) the blue shift of the peak between 1.75 and 2.0 eV from 8-electron systems (β) to 6-electron systems (γ). It is interesting to note that the NIR absorption peak observed at ∼1.1 eV is not the HOMO−LUMO transition but the transition from the HOMO−1 orbital to the LUMO (peak α) as predicted from orbital analysis. The optical HOMO−LUMO transition is forbidden in this case under the dipole selection rule. By contrast, the HOMO−LUMO gaps of 0.32 and 0.29 V for $[PdAu_{24}(SR)_{18}]^0$ and $[PtAu_{24}(SR)_{18}]^0$, respectively, can be readily determined from the voltammograms in Figure 3, offering special advantages in the study of electronic structures near the HOMO−LUMO levels. The splitting of the HOMO manifold was also predicted for $[Au_{25}(SR)_{18}]^+$ in the DFT calculation of $Au_{25}(SR)_{18}$ with different charge states. The prediction was well supported by the electron paramagnetic resonance (EPR) experiments that revealed that the $[Au_{25}(SR)_{18}]^+$ cluster is a diamagnetic species, rather than a paramagnetic diradical cation.[39] In addition, the HOMO−1 is in fact not a superatomic orbital by a hybridization between the icosahedral shell and the ligand layer (Figure S7). Interestingly, the central Au atom in $[Au_{25}(SR)_{18}]^+$ is not involved in the HOMO−1, while Pd and Pt centers are significantly involved in the HOMO−1 (Figure S7).

Is it possible then to form an 8-electron cluster by electronic charging of a 6-electron cluster? The TD-DFT simulation predicts the 8-electron $[PdAu_{24}(SR)_{18}]^{2-}$ and $[PtAu_{24}(SR)_{18}]^{2-}$have an electronic structure very similar to that of $[Au_{25}(SR)_{18}]^-$ and thus would display similar absorption spectra as predicted in Figure 2B. To explore this possibility,

DOI: 10.1021/jacs.5b06946
J. Am. Chem. Soc. 2015, 137, 10833−10840

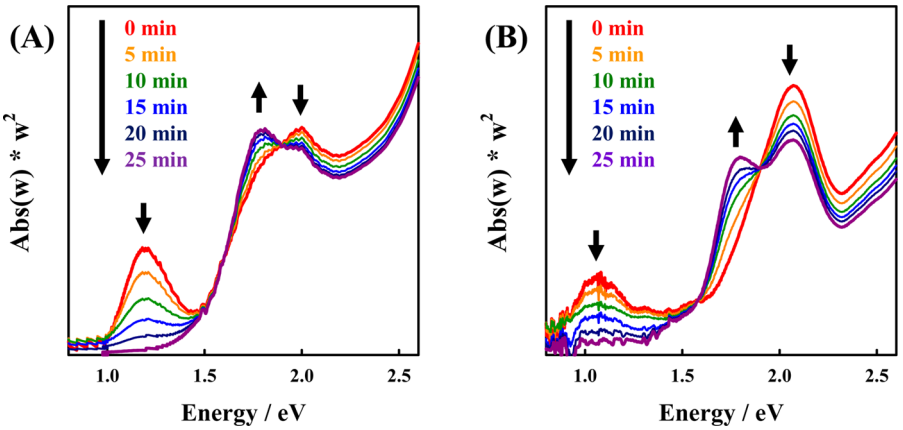

Figure 5. Absorption spectral changes during potentiostatic reduction of (A) $PdAu_{24}(SR)_{18}$ (0.5 mM) and (B) $PtAu_{24}(SR)_{18}$ (0.5 mM) at −1.04 V in CH_2Cl_2 containing Bu_4NPF_6 (0.1 M), TBAB (10 mM), and Oct_4NBr (1.0 mM).

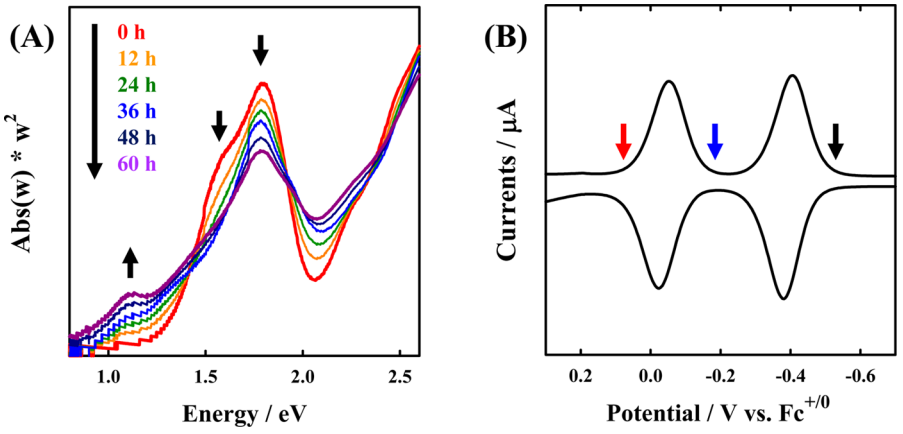

Figure 6. (A) Absorption spectral changes of $Au_{25}(SR)_{18}$ upon chemical oxidation in an ethanol−water/CH_2Cl_2 two-phase mixture for the indicated time. (B) SWV of $Au_{25}(SR)_{18}$ in CH_2Cl_2 containing 0.1 M Bu_4NPF_6. The arrows indicate the OCP of the cluster solution measured after being oxidized for 0 h (black), 36 h (blue), and 60 h (red), corresponding to $[Au_{25}(SR)_{18}]^{-1}$, $[Au_{25}(SR)_{18}]^{0}$, and $[Au_{25}(SR)_{18}]^{+1}$, respectively.

we performed absorption spectroelectrochemistry of $[PdAu_{24}(SR)_{18}]^0$ in CH_2Cl_2 containing 0.1 M Bu_4NPF_6 in an optically transparent thin layer cell. (see the Experimental Section). The $[PdAu_{24}(SR)_{18}]^0$ cluster exhibits a characteristic absorption band at 1.2 eV which is related to the transition involving the P-type LUMO generated in $[PdAu_{24}(SR)_{18}]^0$. There is also an absorption band found at 2.0 eV with a shoulder at ∼1.8 eV. When potential was applied to −1.04 V, at which $[PdAu_{24}(SR)_{18}]^{2-}$ was expected to be the dominant species in the solution, the 1.2 eV band dramatically decreased and disappeared after 25 min (red to purple curve in Figure 5). Whereas the band at 2.0 eV also decreases, a new band at 1.8 eV grows with time. Interestingly, the spectral change observed in Figure 5A is consistent with the change from 6-electron $[PdAu_{24}(SR)_{18}]^0$ to 8-electron $[PdAu_{24}(SR)_{18}]^{2-}$ predicted in Figure 2B; the bands at 1.2, 1.8, and 2.0 eV correspond to respectively α, β, and γ transitions (Figure 4). We note that the electrochemical reduction of $[PdAu_{24}(SR)_{18}]^0$ was carried out in the presence of a mild reducing agent (TBAB) and an appropriate cation such as Oct_4N^+ to stabilize the reduced form, i.e., $[PdAu_{24}(SR)_{18}]^{2-}$. Although the reduction reaction of $[PdAu_{24}(SR)_{18}]^0$ to $[PdAu_{24}(SR)_{18}]^{2-}$ was found to be quite reversible in Figure 3, with potentiostatic reduction alone, the resulting OCP hardly reached below −0.73 V (corresponding to the −1 charge state on average), presumably due to the short lifetime of the $[PdAu_{24}(SR)_{18}]^{2-}$ species. Importantly, the 6-electron system was readily restored upon electrochemical oxidation of $[PdAu_{24}(SR)_{18}]^{2-}$ back to $[PdAu_{24}(SR)_{18}]^0$ (Figure S8A), ensuring that the observed optical changes arise from core-charging, not from cluster degradation. In addition, there are two isosbestic points observed at 1.6 and 1.9 eV, indicating that there are two dominant absorbing species (i.e., $[PdAu_{24}(SR)_{18}]^0$ and $[PdAu_{24}(SR)_{18}]^{2-}$) and the conversion from $[PdAu_{24}(SR)_{18}]^0$ to $[PdAu_{24}(SR)_{18}]^{2-}$ proceeds cleanly without any detectable intermediate species.[30]

$[PtAu_{24}(SR)_{18}]^0$ also displays similar spectral changes upon reduction of $[PtAu_{24}(SR)_{18}]^0$ to $[PtAu_{24}(SR)_{18}]^{2-}$ as shown in Figure 5B. The $[PtAu_{24}(SR)_{18}]^0$ cluster exhibits absorption at 1.1 eV due to the presence of the P-type LUMO. There is another characteristic absorption band at 2.1 eV which involves absorption lines from multiple orbital transitions. Upon potential stepping to −1.04 V (vs $Fc^{+/0}$), where $[PtAu_{24}(SR)_{18}]^0$ was reduced to $[PtAu_{24}(SR)_{18}]^{2-}$, the absorption band at 1.1 eV dramatically decreased and disappeared after 25 min. Additionally, the ∼1.8 eV band grew while the ∼2.0 eV band decreased with time with isosbestic points observed at 1.6 and 1.9 eV. $[PtAu_{24}(SR)_{18}]^0$ was regenerated reversibly upon oxidation of $[PtAu_{24}(SR)_{18}]^{2-}$ back to $[PtAu_{24}(SR)_{18}]^0$ (Figure S8B). Again, these spectral changes evidently suggest that the 6-electron $[PtAu_{24}(SR)_{18}]^0$ became a superatomic 8-electron cluster upon reduction to $[PtAu_{24}(SR)_{18}]^{2-}$. These results clearly show that both $[PdAu_{24}(SR)_{18}]^0$ and $[PtAu_{24}(SR)_{18}]^0$

DOI: 10.1021/jacs.5b06946
J. Am. Chem. Soc. 2015, 137, 10833−10840

clusters adopt stable 6-electron electronic structures and become 8-electron $[Au_{25}(SR)_{18}]^-$-like superatom complexes upon electronic charging.

The above spectroelectrochemistry experiments clearly show that the 6-electron $[PdAu_{24}(SR)_{18}]^0$ ($[PtAu_{24}(SR)_{18}]^0$) becomes a $[Au_{25}(SR)_{18}]^-$-like 8-electron system upon reduction to $[PdAu_{24}(SR)_{18}]^{2-}$ ($[PtAu_{24}(SR)_{18}]^{2-}$). One may question then if the oxidized $[Au_{25}(SR)_{18}]^+$, another 6-electron cluster, would have an electronic structure and absorption spectrum similar to those of $[PtAu_{24}(SR)_{18}]^0$. The spectroelectrochemistry of $[Au_{25}(SR)_{18}]^-$ was, however, unsuccessful because the cluster tends to be decomposed and form a large aggregate under high applied potential (0.010 V vs $Fc^{+/0}$).[39] Instead, we oxidized the $[Au_{25}(SR)_{18}]^-$ cluster chemically in a solution. $[Au_{25}(SR)_{18}]^-$ is known to react with oxygen and be readily oxidized.[40,41] We have also found that the oxidation effectively occurs in the presence of ethanol.[17] Accordingly, the $[Au_{25}(SR)_{18}]^-$ solution in CH_2Cl_2 was added to an ethanol−water mixture, and the resulting two-phase solution was stirred for a long period of time for the oxidation of the $[Au_{25}(SR)_{18}]^-$ cluster. As can be seen in Figure 6, the absorption profile of $[Au_{25}(SR)_{18}]^0$ changed after 36 h of stirring; that is, compared to that of $[Au_{25}(SR)_{18}]^-$, the absorption band at 1.8 eV became weaker and the shoulder peak at 1.6 eV disappeared. These changes are in agreement with the oxidation of $[Au_{25}(SR)_{18}]^-$ to $[Au_{25}(SR)_{18}]^0$.[40−43] The oxidation of $[Au_{25}(SR)_{18}]^-$ to $[Au_{25}(SR)_{18}]^0$ was further confirmed by the OCP measurement (−0.15 V) in Figure 6B.

When the two-phase solution was further stirred for 60 h, the band at 1.8 eV was decreased further and a new band at ∼1.1 eV appeared. While a decrease of the band at 1.8 eV has been observed for the oxidized $[Au_{25}(SR)_{18}]^+$ cluster, the growth of the 1.1 eV absorption peak has never been observed.[44] Interestingly, the peak position is similar to the characteristics of the 6-electron systems, i.e., $[PdAu_{24}(SR)_{18}]^0$ and $[PtAu_{24}(SR)_{18}]^0$. The OCP value was found to be 0.08 V, confirming the formation of $[Au_{25}(SR)_{18}]^+$. These results suggest that $[Au_{25}(SR)_{18}]^-$ becomes a superatomic 6-electron system upon oxidation to $[Au_{25}(SR)_{18}]^+$. When the $[Au_{25}(SR)_{18}]^+$ solution was treated with $NaBH_4$, the spectrum of $[Au_{25}(SR)_{18}]^-$ was almost restored, ensuring that the spectral change was reversible (Figure S8C). Summarizing the spectroelectrochemistry results, superatomic 6-electron clusters such as $[PdAu_{24}(SR)_{18}]^0$ and $[PtAu_{24}(SR)_{18}]^0$ were preferably prepared by replacing the core Au with Pd or Pt. These clusters became superatomic 8-electron clusters by manipulating their oxidation state. By contrast, $Au_{25}(SR)_{18}$ was preferentially prepared as an anionic 8-electron cluster, which underwent geometrical transformation to a $[PdAu_{24}(SR)_{18}]^0$-like, 6-electron system upon oxidation. Reversible interconversion between the 6-electron and 8-electron configurations of $PdAu_{24}(SR)_{18}$, $PtAu_{24}(SR)_{18}$, and $Au_{25}(SR)_{18}$ clusters was clearly demonstrated.

CONCLUSIONS

We have revealed that replacing the core Au atom with Pd or Pt results in stable $[MAu_{24}(SR)_{18}]^0$ clusters (M = Pd, Pt) having a superatomic 6-electron configuration ($1S^21P^4$). These clusters exhibit optical and electrochemical properties drastically different from those of the 8-electron $[Au_{25}(SR)_{18}]^-$ cluster. The HOMO−LUMO gaps of these clusters determined by voltammetry were drastically decreased, indicating their electronic structures were significantly altered upon doping of the foreign metal. These results were strongly supported by the DFT calculations, which also revealed that the MAu_{12} core of the 6-electron $[MAu_{24}(SR)_{18}]^0$ is geometrically distorted, accompanying the 1P orbital splitting. This is the first result showing that Jahn−Teller-like distortion occurs in superatom complexes. Reversible interconversion of the 6-electron and 8-electron configurations of these clusters has been clearly demonstrated by electrochemical manipulation of their oxidation state. The unique electrochemical properties observed from the stable 6-electron clusters suggest that doping of a cluster is a powerful means to fine-tune the redox properties of the cluster, which has practical implications in a variety of electrocatalytic applications.

ASSOCIATED CONTENT

Supporting Information

The Supporting Information is available free of charge on the ACS Publications Web site at ACS Publications website at DOI: 10.1021/jacs.5b06946.

Detailed synthetic procedure and characterization of the clusters and supporting figures and tables (PDF)

AUTHOR INFORMATION

Corresponding Authors

*dongil@yonsei.ac.kr

*de-en.jiang@ucr.edu

Notes

The authors declare no competing financial interest.

ACKNOWLEDGMENTS

D.L. acknowledges support by the Korea CCS R&D Center (KCRC) (Grant NRF-2014M1A8A1074219), NRF Grants NRF-2014R1A2A1A11051032 and 2011-0022975, and the Yonsei University Future-leading Research Initiative of 2014. Computation by DFT (Q.T. and D.-e.J.) was supported by the University of California, Riverside.

REFERENCES

(1) Murray, R. W. *Chem. Rev.* **2008**, *108*, 2688.
(2) Jin, R. *Nanoscale* **2010**, *2*, 343.
(3) Jin, R. *Nanoscale* **2015**, *7*, 1549.
(4) Maity, P.; Xie, S.; Yamauchi, M.; Tsukuda, T. *Nanoscale* **2012**, *4*, 4027.
(5) Meng, X.; Liu, Z.; Zhu, M.; Jin, R. *Nanoscale Res. Lett.* **2012**, *7*, 277.
(6) Heaven, M. W.; Dass, A.; White, P. S.; Holt, K. M.; Murray, R. W. *J. Am. Chem. Soc.* **2008**, *130*, 3754.
(7) Zhu, M.; Aikens, C. M.; Hollander, F. J.; Schatz, G. C.; Jin, R. *J. Am. Chem. Soc.* **2008**, *130*, 5883.
(8) Akola, J.; Walter, M.; Whetten, R. L.; Häkkinen, H.; Grönbeck, H. *J. Am. Chem. Soc.* **2008**, *130*, 3756.
(9) Parker, J. F.; Fields-Zinna, C. A.; Murray, R. W. *Acc. Chem. Res.* **2010**, *43*, 1289.
(10) Walter, M.; Akola, J.; Lopez-Acevedo, O.; Jadzinsky, P. D.; Calero, G.; Ackerson, C. J.; Whetten, R. L.; Grönbeck, H.; Häkkinen, H. *Proc. Natl. Acad. Sci. U. S. A.* **2008**, *105*, 9157.
(11) Tofanelli, M. A.; Ackerson, C. J. *J. Am. Chem. Soc.* **2012**, *134*, 16937.
(12) Negishi, Y.; Nobusada, K.; Tsukuda, T. *J. Am. Chem. Soc.* **2005**, *127*, 5261.
(13) Park, S.; Lee, D. *Langmuir* **2012**, *28*, 7049.
(14) Kim, J.; Lema, K.; Ukaigwe, M.; Lee, D. *Langmuir* **2007**, *23*, 7853.

DOI: 10.1021/jacs.5b06946
J. Am. Chem. Soc. 2015, 137, 10833−10840

(15) Lee, D.; Donkers, R. L.; Wang, G.; Harper, A.; Murray, R. W. *J. Am. Chem. Soc.* **2004**, *126*, 6193.
(16) Guo, R.; Murray, R. W. *J. Am. Chem. Soc.* **2005**, *127*, 12140.
(17) Kwak, K.; Lee, D. *J. Phys. Chem. Lett.* **2012**, *3*, 2476.
(18) Negishi, Y.; Iwai, T.; Ide, M. *Chem. Commun.* **2010**, *46*, 4713.
(19) Kauffman, D. R.; Alfonso, D.; Matranga, C.; Qian, H.; Jin, R. *J. Phys. Chem. C* **2013**, *117*, 7914.
(20) Kumara, C.; Aikens, C. M.; Dass, A. *J. Phys. Chem. Lett.* **2014**, *5*, 461.
(21) Negishi, Y.; Munakata, K.; Ohgake, W.; Nobusada, K. *J. Phys. Chem. Lett.* **2012**, *3*, 2209.
(22) Xie, S.; Tsunoyama, H.; Kurashige, W.; Negishi, Y.; Tsukuda, T. *ACS Catal.* **2012**, *2*, 1519.
(23) Niihori, Y.; Kurashige, W.; Matsuzaki, M.; Negishi, Y. *Nanoscale* **2013**, *5*, 508.
(24) Miller, S. A.; Fields-Zinna, C. A.; Murray, R. W.; Moran, A. M. *J. Phys. Chem. Lett.* **2010**, *1*, 1383.
(25) Qian, H.; Barry, E.; Zhu, Y.; Jin, R. *Acta Phys. Chim. Sin.* **2011**, *27*, 513.
(26) Fields-Zinna, C. A.; Crowe, M. C.; Dass, A.; Weaver, J. E.; Murray, R. W. *Langmuir* **2009**, *25*, 7704.
(27) Negishi, Y.; Kurashige, W.; Niihori, Y.; Iwasa, T.; Nobusada, K. *Phys. Chem. Chem. Phys.* **2010**, *12*, 6219.
(28) Jiang, D.; Dai, S. *Inorg. Chem.* **2009**, *48*, 2720.
(29) Kacprzak, K. A.; Lehtovaara, L.; Akola, J.; Lopez-Acevedo, O.; Häkkinen, H. *Phys. Chem. Chem. Phys.* **2009**, *11*, 7123.
(30) Negishi, Y.; Kurashige, W.; Kobayashi, Y.; Yamazoe, S.; Kojima, N.; Seto, M.; Tsukuda, T. *J. Phys. Chem. Lett.* **2013**, *4*, 3579.
(31) Qian, H.; Jiang, D. E.; Li, G.; Gayathri, C.; Das, A.; Gil, R. R.; Jin, R. *J. Am. Chem. Soc.* **2012**, *134*, 16159.
(32) Christensen, S. L.; MacDonald, M. A.; Chatt, A.; Zhang, P.; Qian, H.; Jin, R. *J. Phys. Chem. C* **2012**, *116*, 26932.
(33) Ahlrichs, R.; Bar, M.; Haser, M.; Horn, H.; Kolmel, C. *Chem. Phys. Lett.* **1989**, *162*, 165.
(34) Andrae, D.; Haussermann, U.; Dolg, M.; Stoll, H.; Preuss, H. *Theor. Chim. Acta* **1990**, *77*, 123.
(35) Tao, J.; Perdew, J. P.; Staroverov, V. N.; Scuseria, G. E. *Phys. Rev. Lett.* **2003**, *91*, 146401.
(36) Wolter, S. D.; Brown, I. B.; Parker, C. B.; Stoner, B. R.; Glass, J. T. *Appl. Surf. Sci.* **2010**, *257*, 1431.
(37) Jiang, Z.; Zhang, W.; Jin, L.; Yang, X.; Xu, F.; Zhu, J.; Huang, W. *J. Phys. Chem. C* **2007**, *111*, 12434.
(38) MacDonald, M. A.; Zhang, P.; Qian, H.; Jin, R. *J. Phys. Chem. Lett.* **2010**, *1*, 1821.
(39) Antonello, S.; Perera, N. V.; Ruzzi, M.; Gascón, J. A.; Maran, F. *J. Am. Chem. Soc.* **2013**, *135*, 15585.
(40) Zhu, M.; Eckenhoff, W. T.; Pintauer, T.; Jin, R. *J. Phys. Chem. C* **2008**, *112*, 14221.
(41) Kauffman, D. R.; Alfonso, D.; Matranga, C.; Li, G.; Jin, R. *J. Phys. Chem. Lett.* **2013**, *4*, 195.
(42) Venzo, A.; Antonello, S.; Gascón, J. A.; Guryanov, I.; Leapman, R. D.; Perera, N. V.; Sousa, A.; Zamuner, M.; Zanella, A.; Maran, F. *Anal. Chem.* **2011**, *83*, 6355.
(43) Zhu, M.; Chan, G.; Qian, H.; Jin, R. *Nanoscale* **2011**, *3*, 1703.
(44) Negishi, Y.; Chaki, N. K.; Shichibu, Y.; Whetten, R. L.; Tsukuda, T. *J. Am. Chem. Soc.* **2007**, *129*, 11322.

DOI: 10.1021/jacs.5b06946
J. Am. Chem. Soc. 2015, 137, 10833−10840